 doi:10.20944/preprints202210.0349.v1

Article

Using Various Analysis Center Products to Assess the Time-Frequency Transfer Performance of GPS/Galileo/BDS PPPAR Methods

Mingjun Ouyang[1,2], Xiangwei Zhu [1,2,3,*], Ruite Yi [2,3], Daqian Lyu[4]

1. School of Electronics and Communication Engineering, Sun Yat-Sen University, Guangzhou 510006, China;
2. Shenzhen Key Laboratory of navigation and communication integration, Shenzhen, China;
3. School of System Science and Engineering Sun Yat-Sen University, Guangzhou 510006, China;
4. College of Electronic Engineering, National University of Defense Technology, Hefei 230037, China.

* Correspondence: zhuxw666@mail.sysu.edu.cn.

Abstract: These days, numerous organizations and Analysis Centers (AC) offer various Ambiguity Resolution (AR) products using various methodologies. To use it for time-frequency transfer, there is no associated study. This paper chooses 16 Multi-GNSS Experiment (MGEX) stations with external high-precision atomic clocks to constitute 15 international time comparison links and uses AR products data from CNES, SGG, CODE, and PRIDE laboratory, using three ambiguity-fixed strategies, to thoroughly evaluate the effects of various strategies and AR products for high-precision time-frequency transfer. We reach the following results by using the IGS final clock product as a reference and comparing it to ambiguity-float. With various ambiguity-fixed procedures, the time stability Standard Deviation (STD) of time transfer is increased for a single GPS, and the improvement ranges from 10% to 40%. The frequency stability has barely improved; up to 40%, the most notable improvement comes from FCB with GRM products. The time stability STD of combinations has improved after the addition of the Galileo system compared to the single GPS, and the improvement ranges from 2% to 9%. Most strategies have been improved, while a few techniques have weakened with the GEC (GPS+Galileo+BDS) combination. We feel that the stability has not significantly increased with the system's increase within short-term stability after comparing multiple groups of linkages.

Keywords: Time Frequency Transfer; Precise Point Positioning; Ambiguity Resolution (AR); Analysis Center (AC)

1. Introduction

Common View (CV) [1-3], All in View (AV) [4-6], Precise Point Positioning (PPP) [4, 7], and Two-Way Satellite Time and Frequency Transfer (TWSTFT) [8] are some of the current GNSS time transfer techniques. Since September 2009, GPS PPP has been a crucial approach in the International Atomic Time (TAI) time comparison [5, 7]. The GNSS PPP technique has the advantages of globalization, all-weather, high precision, and low cost, and its short-term stability is superior to that of TWSTFT. Its time transfer accuracy is also comparable to that of TWSTFT. One of the current hot topics in high-precision time transfer technology is the GNSS PPP approach.

Time-frequency transfer is done via pseudo-range and carrier phase observations in GNSS PPP approaches [9]. Better short-term stability can be attained compared to pseudo-range only techniques because phase observations have lower noise levels and higher measurement precision [10]. According to pertinent studies, the normal uncertainty of PPP frequency comparisons has an average day stability of roughly 1×10^{-15} and stability of 1×10^{-16} over a 30-day period. The Type A uncertainty of Circular T for the time comparison link of the BIPM is less than 0.3 ns [7].

 doi:10.20944/preprints202210.0349.v1

The PPP approach was first employed for high precision positioning [11] before being widely applied in the monitoring of crustal deformation [12], meteorology [13], high precision dynamic positioning [14], and monitoring of local seismic activity [15].

Recent advances in PPP ambiguity-fixed technology have significantly increased convergence speed, positioning accuracy, and stability. Scholars and research organizations both domestically and abroad, have given it considerable attention. The ambiguity-fixed solution PPP has distinct advantages over the ambiguity-float solution PPP, because when the ambiguity converges or has a certain accuracy, it fully utilizes the integer advantage of ambiguity to convert the phase observation value that contains ambiguity into a high-precision absolute distance observation value, which quickly increases the positioning accuracy to a stable centimeter level. Because they do not adequately handle the deviation terms contained in the observed values from the model, much earlier research has concentrated on ambiguous float solution PPP. These deviation terms contaminate the ambiguity and render it unfixable. Although numerous PPP ambiguity-fixed approaches have been devised, their overarching objective is reinstating ambiguity's fixable (integer) characteristic.

Three representative PPP ambiguity-fixed methods have been proposed: the integer phase clock method by Laurichesse et al. of the CNES (Centre National d'Etudes Spatials) in France [17], the decimal deviation method by Ge et al. of the GFZ (Geo Forschungs Zentrum) in Germany [16], and the clock difference decoupling method by Collins et al. of NRCan (Natural Resources Canada). Domestic researchers have noted that these methods are equivalent from a variety of perspectives but have also noted that they differ in the final products and algorithm implementation [19, 20]. The observable-specific signal bias (OSBs) in Solution INdependent EXchange (SINEX) format, which includes the observable-specific satellite code and phase bias corrections for each frequency, can be directly applied to the raw observations before forming any linear combination.

Some institutions are currently able to offer PPP AR products for the GPS, Galileo, and BDS systems. The benefits of various institutional products and various system products are therefore worth additional comparison and analysis, and then further examination of the impact of its applications, to sort out the multi-GNSS (GPS, Galileo, BDS) PPP AR (whether it is positioning or time transfer applications). There is currently no research on time-frequency transfer, and the performance of various PPP AR products from various institutions has only been studied in terms of locating applications [21, 22].

More than 80% of independent ambiguities can be consistently addressed, according to experimental findings in the literature [16], and the PPP single-day static solution with fixed ambiguity in the east direction has a positioning accuracy of about 30% greater than the PPP's actual solution. The U direction and the clock difference parameter are correlated, as demonstrated in related research [23], eliminating any remaining uncertainty. This strengthens the position of the U direction and, in turn, the clock difference parameter.

In less than a week of solution time, the first PPPAR experiment for time-frequency transfer demonstrated that frequency stability of 1×10^{-16} was possible with PPPAR technology [10]. The GRE PPPAR mode watches the clock when RT-IPPP technology is used, detecting changes with a frequency larger than 6.1×10^{-15} [24]. Their effort is limited to a single source AR product and a single ambiguity fixing method.

This work performs high-precision time-frequency transfer experiments with AR products from CNES, SGG, CODE, and PRIDE laboratories using three ambiguity-fixed techniques. A thorough investigation of the time-frequency transfer theory and associated GPS/Galileo/BDS PPPAR technique results for various analysis center products is carried out using the IGS 30-second final clock difference product as a reference.

The structure of the article is as follows: The PPPAR time transfer principle and function model are initially introduced; the experimental data and comprehensive processing

Preprints (www.preprints.org) | NOT PEER-REVIEWED | Posted: 24 October 2022 doi:10.20944/preprints202210.0349.v1

schemes are then presented; Compare and demonstrate the utilization of several techniques when in static mode. Performance outcomes for numerous goods using multi-GNSS PPP AR time-frequency transmission; Give a summary and draw conclusions.

2. Materials and Methods

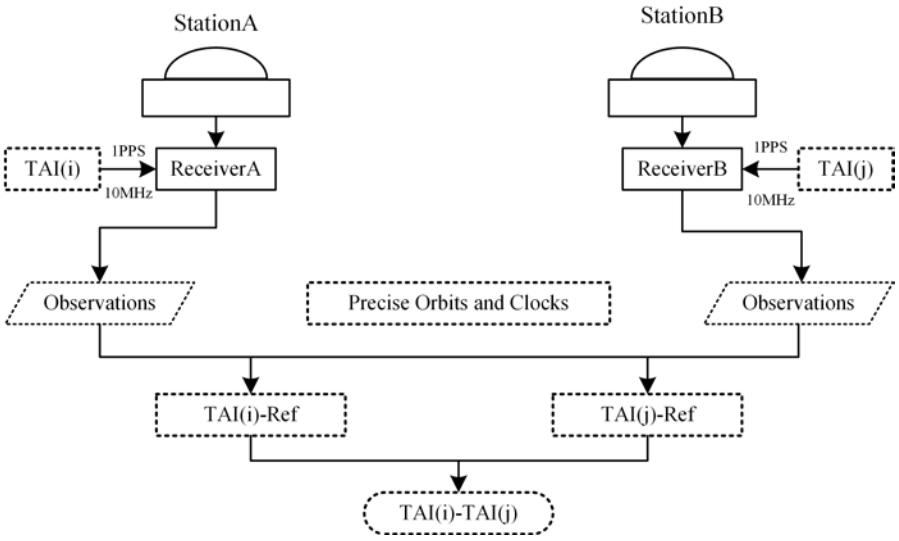

Figure 1. Sketch map for PPPAR time-frequency transfer

2.1 PPPAR Time transfer

The stations are typically coupled to high-precision time-frequency reference signals (1PPS and 10MHZ) for the high-precision time-frequency transfer of the PPPAR approach, like stations A and B in Figure 1 above. The station leverages precision products produced outside to collect pseudo-range and carrier phase observation data through the GNSS antenna (precision orbit, clock difference, DCB, AR products, etc.). The calibration of the hardware delay is completed by determining the difference between the clocks CLK(a) and CLK(b) connected to the receiver and the standard reference time (such as GPST, IGST, or UTC (NTSC)), performing the difference operation to obtain that difference, and then passing the calibration method. Gets the local atomic clock difference to match the PPPAR process's time-frequency transmission. This paper's clock difference is the outcome of ambiguity-fixed technology, which typically uses PPP technology. The alternative approach is as follows:

$$\text{CLK(a)-CLK(b)=(CLK(a)-Ref) - (CLK(b)-Ref)} \quad (1)$$

2.2 GNSS-PPPAR model

The formula examples illustrate the main observations of GNSS raw pseudo-range and phase:

$$\begin{cases} P_{r,j} = \rho_r + dt_r - dt^s + m_{w,r}T_{w,r} + \gamma_j I_{r,1} + b_{r,j} + b_j^s + \varepsilon_{P_j} \\ L_{r,j} = \rho_r + dt_r - dt^s + m_{w,r}T_{w,r} + \gamma_j I_{r,1} + \lambda_j N_{r,j} + B_{r,j} + B_j + \varepsilon_{L_j} \end{cases} \quad (2)$$

P represents pseudo-range observations; L represents carrier phase observations; r and j represent receiver and signal frequency, respectively; ρ represents the geometric distance between the satellite and the receiver; $T_{w,r}$ represents the tropospheric Zenith Wet Delay (ZWD); I represents ionospheric delay; $\gamma_j = (f_1 / f_j)^2$ and f_j represents frequency j coefficient; dt_r and dt^s represents receiver and satellite clock difference, re-

Preprints (www.preprints.org) | NOT PEER-REVIEWED | Posted: 24 October 2022 doi:10.20944/preprints202210.0349.v1

spectively; $m_{w,r}$ representing map projection function; $N_{r,j}$ is the integer phase ambiguity; λ_j means wavelength in frequency *j*; $\varepsilon^s_{P_j}$ and $\varepsilon^s_{L_j}$ are the pseudo-range and carrier phase error term which did not quantize into the function model, respectively. The observable-specific signal bias (OSBs), which includes the observable-specific satellite code and phase bias corrections for each frequency, can be directly applied to the raw observations before forming any linear combination. This method of directly fixed method of the ambiguity is called OSB.

$b_{r,j}$ and $B_{r,j}$ are the Uncalibrated Code Delay (UCD) and Uncalibrated Phase Delay (UPD) at the receiver; b^s_j and B^s_j are UCD and UPD at the satellite end. The general function model is the combination of Ionospheric-Free (IF). We define the coefficient as follows:

$$\alpha_{ij} = \frac{(f_i)^2}{(f_i)^2 - (f_j)^2}, \beta_{ij} = -\frac{(f_j)^2}{(f_i)^2 - (f_j)^2} \tag{3}$$

We assume that:

$$\begin{cases} b_{r,j} = \Delta b_{r,j} + \delta b_{r,j} \\ b^s_j = \Delta b^s_j + \delta b^s_j \\ B_{r,j} = \Delta B_{r,j} + \delta B_{r,j} \\ B^s_j = \Delta B^s_j + \delta B^s_j \end{cases} \tag{4}$$

Δ and δ represent constant and variable parts of hardware delay, respectively [25]. IF combined pseudo-range and carrier observations can be written as follows:

$$P_{r,IF} = \alpha_{12} P_{r,1} + \beta_{12} P_{r,2} = \rho_r + dt_r - dt^s + m_{w,r} T_{w,r} + b_{r,IF} + b^s_{IF} + \varepsilon_{P_{IF}} \tag{5}$$

$$L_{r,IF} = \alpha_{12} L_{r,1} + \beta_{12} L_{r,2} = \rho_r + dt_r - dt^s + m_{w,r} T_{w,r} + N^s_{r,IF} + B_{r,IF} + B^s_{IF} + \varepsilon_{L_{IF}} \tag{6}$$

$$N^s_{r,IF} = \lambda_{NL} N^s_{r,1} - \frac{\lambda_2}{\gamma_2 - 1} N^s_{r,WL} \tag{7}$$

$N_{r,WL}$ is the Wide-Lane (WL) ambiguity and λ_{NL} is the wavelength of the narrow-lane (NL) ambiguity, so herein $N^s_{r,1}$ is called the NL ambiguity. Meanwhile, we have the Hatch-Melbourne–Wubbena (HMW) combination as follows:

$$\mathrm{K}_{MW} = \lambda_{WL}\left(\frac{L_1}{\lambda_1} - \frac{L_2}{\lambda_2}\right) - \frac{f_1 P_1 + f_2 P_2}{f_1 + f_2}$$

$$= \lambda_{WL} N^s_{r,WL} + \tau_{r,WL} + \tau^s_{WL} \tag{8}$$

λ_{WL} is the WL wavelength. To eliminate the hardware delay at the receiver, PPPAR generally uses the method of an inter-satellite single difference (SD). The ambiguity of SD IF combination and WL ambiguity is expressed as follows:

$$\begin{cases} N^{ij}_{r,IF} = N^i_{r,IF} - N^j_{r,IF} \\ N^{ij}_{r,WL} = N^i_{r,WL} - N^j_{r,WL} \end{cases} \tag{9}$$

Generally, the IGS satellite clock difference product absorbs the pseudo-range hardware delay. The satellite clock difference can be expressed as follows:

$$\begin{cases} dt^s_{P_{IF}} = dt^s - \Delta b^s_{IF} - \delta B^s_{IF} \\ b^s_{IF} = \alpha_{12} b^s_1 + \beta_{12} b^s_2 \end{cases} \tag{10}$$

$dt^s_{P_{IF}}$ represents satellite clock difference products, and dt^s represents the "real" clock difference of satellite clock. To make use of this IF satellite clock product, we rewrite (10) as :

Preprints (www.preprints.org) | NOT PEER-REVIEWED | Posted: 24 October 2022 doi:10.20944/preprints202210.0349.v1

$$\begin{cases} dt^s + \Delta b_1^s = dt_{P_{IF}}^s + \beta_{12} DCB_{12}^s \\ dt^s + \Delta b_2^s = dt_{P_{IF}}^s - \alpha_{12} DCB_{12}^s \end{cases} \tag{11}$$

DCB_{ij}^s is the DCB at the satellite end, which is $\Delta b_i^s - \Delta b_j^s$, we can obtain the data from CODE. Substitute clock difference to obtain:

$$P_{IF} = \rho_r + dt_{r,P_{IF}} + m_{w,r} T_{w,r} + \Psi + \varepsilon_{P_{IF}}$$

$$L_{IF} = \rho_r + dt_{r,P_{IF}} + m_{w,r} T_{w,r} + N_{r,IF}^s + \Delta B_{r,IF} - \delta b_{r,IF} + \Delta B_{IF}^s + \Delta b_{IF}^s + \varepsilon_{L_{IF}} \tag{12}$$

with：

$$\begin{cases} dt_{r,P_{IF}}^s = dt_r^s + \Delta b_{r,IF}^s + \delta B_{r,IF}^s \\ \Psi = \delta b_{r,IF}^s - \delta B_{r,IF}^s + \delta b_{IF}^s + \delta B_{IF}^s \\ N_{r,IF}^s = N_{r,IF}^s + \Delta B_{IF}^s + \Delta b_{IF}^s + \Delta B_{r,IF}^s - \Delta b_{r,IF}^s \end{cases} \tag{13}$$

Θ will be submerged by pseudo-range noise and finally enter the pseudo-range residual. The IF combination's ambiguity is divided into a linear combination of WL and NL in formula (7). The WL is fixed first, followed by the NL, in the fixed ambiguity sequence. Following are the fixed stages [26]:

Firstly, determine the SD IF float ambiguity. Calculate the ambiguity parameters and the accompanying Variance-Covariance Matrix (VCM) by applying the error propagation approach to the standard extended Kalman filter (EKF) calculation:

$$\begin{cases} N_{r,IF}^{ij} = N_{r,IF}^i - N_{r,IF}^j = N_{r,IF}^{ij} + \left[\Delta B_{IF}^{ij} \right] + \left[\Delta b_{IF}^i \right] \\ Q_{N_{r,IF}^{ij}} = \left(H_{SD} Q_{N_{r,IF}} H_{SD}^T \right)_{ij} \end{cases} \tag{14}$$

$N_{r,IF}^{ij}$ is a SD IF solution. With their variance denoted by $Q_{N_{r,IF}^{ij}}$, H_{SD} is SD design matrix and $Q_{N_{r,IF}}$ is IF ambiguity VCM calculated by EKF. The symbol [·] indicates that this term can be eliminated by using CODE and WHU PPPAR products.

Secondly, fixed SD WL ambiguity. The MW combination can be used to calculate the float solution to the WL ambiguity. The (OBS or FCB) product can then be used to obtain the integer solution. In general, it can also be rounded up directly.

$$\hat{N}_{r,WL}^{ij} = round\left(\left(\overline{\Psi}_{mw}^{ij} + \left[\tau_{WL}^{ij} \right] \right) / \lambda_{WL} \right) \tag{15}$$

$\hat{N}_{r,WL}^{ij}$ denotes fixed SD WL ambiguity and represents the average MW combination; the WL UPD correction is dispensable and can be eliminated using CODE and WHU PPPAR products.

Thirdly, the SD NL ambiguity was fixed. Following a successful WL ambiguity correction, the expression equation for the SD NL term can be written as follows:

$$\begin{cases} \tilde{N}_{r,1}^{ij} = \left(\tilde{N}_{r,IF}^{ij} + \dfrac{\lambda_2}{\gamma_2 - 1} N_{r,WL}^{ij} + \left[\tau_{NL}^{ij} \right] \right) / \lambda_{NL} \\ Q_{\tilde{N}_{r,1}^{ij}} = \left(\dfrac{1}{(\lambda_{NL})^2} Q_{\tilde{N}_{r,IF}} \right)_{ij} \end{cases} \tag{16}$$

$Q_{\tilde{N}_{r,1}^{ij}}$ the SD float NL ambiguities are obtained by applying the covariance propagation law. The NL UPD correction τ_{NL}^{ij} is required for the FCB method. Since NL ambiguities are strongly correlated in PPP, the popular Least-squares Ambiguity Decorrelation Adjustment (LAMBDA) method or a modified variant serves as the foundation of a search strategy. The widely used ratio test and success rate are used to decide what has to be fixed.

Fourthly, Fixed SD IF composition. After the SD WL and NL are successfully fixed, the SD ionospheric combination can be recalculated to obtain:

Preprints (www.preprints.org) | NOT PEER-REVIEWED | Posted: 24 October 2022 doi:10.20944/preprints202210.0349.v1

$$\hat{N}_{r,IF}^{ij} = \lambda_{NL}^{s}\left(\hat{N}_{r,1}^{ij} - \left[\tau_{NL}^{ij}\right]\right) - \frac{\lambda_2^s}{\gamma_2^s - 1}\hat{N}_{r,WL}^{ij} \quad (17)$$

NL UPD correction τ_{NL}^{ij} is required for the FCB method.

Lastly, Update the fixed solution. Other parameters can be updated by their correlation with fixed ambiguities, such as location, ZWD, the clock difference parameters, and the remaining unfixed ambiguities addressed in this paper:

$$\hat{b} = \tilde{b} - Q_{\hat{b}\hat{N}}Q_{\tilde{N}}^{-1}\left(\hat{N} - \tilde{N}\right) \quad (18)$$

$\hat{b}$ and $\tilde{b}$ are fixed and unfixed parameters, respectively, $\tilde{N}$ is float solution and the corresponding covariance matrix VCM $Q_{\tilde{N}}^{-1}$, $\hat{N}$ is the integer ambiguity vector, $Q_{\hat{b}\hat{N}}$ is the covariance matrix of $\hat{b}$ and $\hat{N}$.

The receiver clock difference parameters in this paper are updated using

$$\hat{b} = \left(\hat{pos}, \hat{clk}, \hat{ZWD}, \hat{N_{unfix}}\right) \quad (19)$$

Formula (19) contains the position $\hat{pos}$, zenith tropospheric delay ZWD, the clock difference parameters $\hat{clk}$, and the remaining unfixed ambiguity N_{unfix}. $\hat{clk}$ are the clock difference solved in this paper, which is the parameters after the ambiguity is fixed.

In order to create 15 international time comparison links, this paper chooses 16 MGEX stations with external high-precision atomic clocks, uses AR product data from CNES, SGG, CODE, and PRIDE laboratory, and conducts high-precision time-frequency transfer experiments using three ambiguity-fixed strategies. Using the IGS final clock product as a benchmark and contrasting it with ambiguity-float.

3. Experimental data and processing strategies

The Bureau International des Poids et Measures (BIPM) was established in 1975 with the primary goal of ensuring the standardization of time measurement worldwide. The information from more than 500 atomic clocks provided by BIPM at time laboratories across the world is weighted to produce International Atomic Time (TAI). The PTB (Physikalisch-Technische Bundesanstalt) in Germany serves as the key node for the current international time comparison [27].

The chosen stations are primarily based on the following criteria: they must be participating stations in the BIPM international time comparison time laboratory, have a receiver attached to an ultra-reliable atomic clock, and have at least GPS, Galileo, and BDS system observations. Figure 2 illustrates the selection of experimental observation data from 16 globally dispersed sites. The MGEX FTP server served as the source of the observation data. Table 1 displays the specific setup information for these stations, including antennas and the different kinds of external atomic clocks.

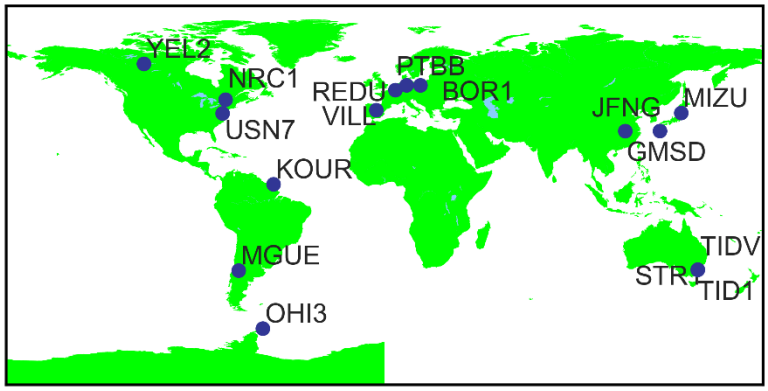

Figure 2. The distribution map of 16 stations was selected, and each station is externally connected with a high-precision atomic clock.

Preprints (www.preprints.org) | NOT PEER-REVIEWED | Posted: 24 October 2022 doi:10.20944/preprints202210.0349.v1

Table 1. 16 stations selected detailed configuration information table (from igs.org)

	site	external source	receiver	antenna
1	BOR1	EXTERNAL H-MASER	TRIMBLE NETR9	TRM59800.00
2	GMSD	EXTERNAL CESIUM	TRIMBLE NETR9	TRM59800.00
3	JFNG	INTERNAL	TRIMBLE ALLOY	TRM59800.00
4	KOUR	EXTERNAL H-MASER	SEPT POLARX5	SEPCHOKE_B3E6
5	MGUE	SEPT POLARX5TR	LEIAR25.R4	EXTERNAL H-MASER
6	MIZU	INTERNAL	SEPT ASTERX4	SEPCHOKE_B3E47
7	NRC1	EXTERNAL H-MASER	JAVAD TRE_G3TH DELTA	SEPCHOKE_B3E37
8	OHI3	EXTERNAL H-MASER	LEICA GR50	SEPCHOKE_B3E49
9	REDU	EXTERNAL CESIUM	SEPT POLARX5	SEPCHOKE_B3E102
10	STR1	EXTERNAL CESIUM	SEPT POLARX5	SEPCHOKE_B3E151
11	VILL	EXTERNAL CESIUM	SEPT POLARX5	SEPCHOKE_B3E6
12	YEL2	EXTERNAL VCH-1008 MASER	SEPT POLARX5TR	LEIAR25.R4
13	USN7	EXTERNAL H-MASER	SEPT POLARX5TR	TPSCR.G5
14	PTBB	EXTERNAL ACTIVE H-MASER	SEPT POLARX5TR	SEPCHOKE_B3E89
15	TIDV	EXTERNAL H-MASER	SEPT POLARX5	SEPCHOKE_B3E169
16	TID1	EXTERNAL H-MASER	SEPT POLARX5	SEPCHOKE_B3E169

The publicly accessible PPPAR solutions produced by several agencies with three preset strategies are listed in Table 2. For the sake of conciseness, the terms "GRM", "WUM", "COM," and "WHU" in the remaining sections of this article, respectively, stand for PPP AR products from CNES, SGG-WHU, CODE, and PRIDE Lab. BDS-2 and QZSS FCB products are provided by SGG-WHU, and PRIDE Labs supports BDS-2 and BDS-3 satellites for PPPAR [22]. This article's data is based on information as of January 1, 2020. These three fixed techniques are referred to as FCB, IRC, and observable-specific code biases (OSBs) in the article that follows.

Table 2. An overview of the PPP AR products [22]

Agency	Strategy	Constellation
CNES	IRC	GRE
WUM	FCB	GREB2J
CODE	OSBs	GREB2*
PRIDE	OSBs	GREB2B3

4. PPP detailed processing strategy

The detailed PPPAR strategy of the article is shown in Table 3 below:

Preprints (www.preprints.org) | NOT PEER-REVIEWED | Posted: 24 October 2022 doi:10.20944/preprints202210.0349.v1

Table 3. PPPAR Detailed Policy

Project	Strategy
Stations	16 globally distributed MGEX stations
Period	January 2020, DOY 001
Observations	GPS: L1, L2 and Galileo: E1, E5a BDS: B1I, B3I
Interval	30 s
Weighting	sin elev^2, cut-off angle 7°
Phase wind-up	Phase wind-up Corrected
Tropospheric delay（ZHD）	Global Pressure and Temperature (GPT)[28] model using the formulas of Saastamoinen
Tropospheric delay（ZWD）	Estimated as a continuous piecewise linear function (2h parameter spacing), GMF mapping function [29]
Tidal displacements	IERS conventions 2010 [30]
Relativistic effect	Corrected
Sagnac	Corrected
Satellite antenna PCOs and PCVs	Fixed to the values from igs14.atx

It should be noted that this study employs the Kalman filtering technique. As a result, the PPP outcomes at the initialization stage were not significant. The PPP results are smoothed in this research by combining forward and reverse filtering with smoothing. Three steps make up the process: forward PPP filtering results, reverse PPP filtering results, and combining the first two results using the weighted average approach. This smoothing equation has the following form:

$$\begin{aligned} Q_k^{result} &= \left(\left(Q_k^f\right)^{-1}+\left(Q_k^b\right)^{-1}\right)^{-1} \\ \boldsymbol{X}_k^{result} &= Q_k^{result}\cdot\left(\left(Q_k^f\right)^{-1}\cdot\boldsymbol{X}_k^f+\left(Q_k^b\right)^{-1}\cdot\boldsymbol{X}_k^b\right). \\ &= \boldsymbol{X}_k^f+Q_k^{result}\cdot\left(Q_k^f\right)^{-1}\cdot\left(\boldsymbol{X}_k^b-\boldsymbol{X}_k^f\right) \end{aligned} \tag{19}$$

Q_k^f and $\boldsymbol{X}_k^f$ are the variance matrix and state vector at time k, respectively. Q_k^b and $\boldsymbol{X}_k^b$ are corresponding to the forward filtering result at time k, and are respectively the variance matrix and state vector corresponding to the reverse filtering result at time k; Q_k^{result} and $\boldsymbol{X}_k^{result}$ are the variance matrix and state vector corresponding to the smoothed result at time k, respectively. The convergence time issue in the first stage of PPP or PPPAR is eliminated in this research using the bidirectional Kalman filter approach.

5. Validation and analysis

5.1. Test case

The ambiguity-fixed methods FCB, IRC, and OSB are all three of them. Due to the existence of precision orbit and clock products with various analysis centers, we use three fixed methods (FCB, IRC, and OSB) to create a system of six alternative ways to study our results. The following six categories for numerous items are determined by three approaches (FCB, IRC, and OSB), as indicated in Table 4:

Table 4. 6 ways of 3 fixed strategies measures taken in this paper

Preprints (www.preprints.org) | NOT PEER-REVIEWED | Posted: 24 October 2022 doi:10.20944/preprints202210.0349.v1

FCB	FCB-com FCB-gbm FCB-grm
IRC	IRC-grm
OSB	OSB-com OSB-whu

There is no convergence issue with the PPP approach because we employ the bidirectional filtering method for better analysis and comparison. The positioning outcome of the PTBB station is depicted in Figure 3. It is obvious that there is no convergence issue and that the convergence effect may always be obtained. It consistently maintains a 1 cm accuracy in three directions (NEU). Later, we all use this technique.

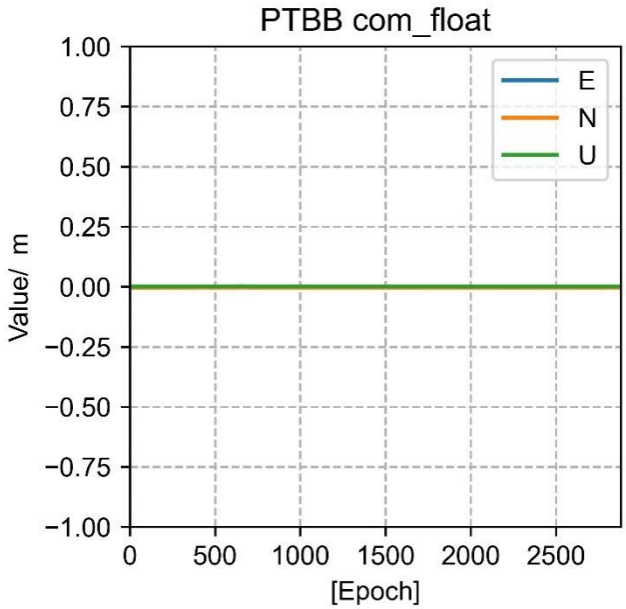

Figure 3. Position results of bidirectional filtering of PTBB station

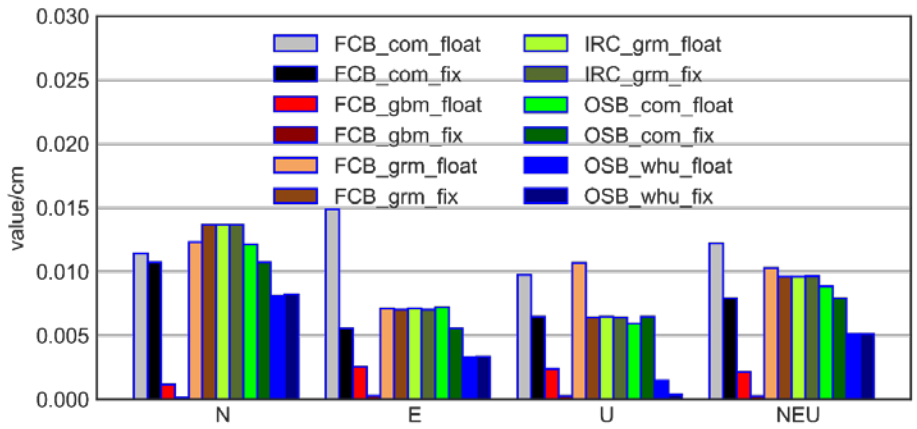

Figure 4. 6 ways of 3 fixed strategies (FCB, IRC, OSB) positioning results, includes three directions of NEU and RMS value composed of three directions.

Preprints (www.preprints.org) | NOT PEER-REVIEWED | Posted: 24 October 2022 doi:10.20944/preprints202210.0349.v1

Using various analysis center products, some academics have carried out positioning work [21, 22]. To help with a better grasp of the overall logic, we also do the positioning results here. Three directions are divided (NEU), and the RMS display is displayed in Figure 4. We can observe that the ambiguity-fixed has a positive effect on the positioning if we use the SNX weekly solution as a point of reference. After the ambiguity is resolved, nearly all solutions produce superior positioning outcomes. The performance of GBM is the finest among them, and the localization outcomes are exceptional.

We are aware that there is a strong association between the U direction and clock difference [23]. We assume that the clock difference operates more effectively because the U direction is enhanced. On the basis of this concept, we continue to solve the clock difference result after the ambiguity has been resolved. With 16 stations, it is clear that ambiguity-fixed is quite effective at containing those floating out points. Here, we list a website: Figure 5 displays 3 PTBB station techniques (FCB, IRC, and OSB).

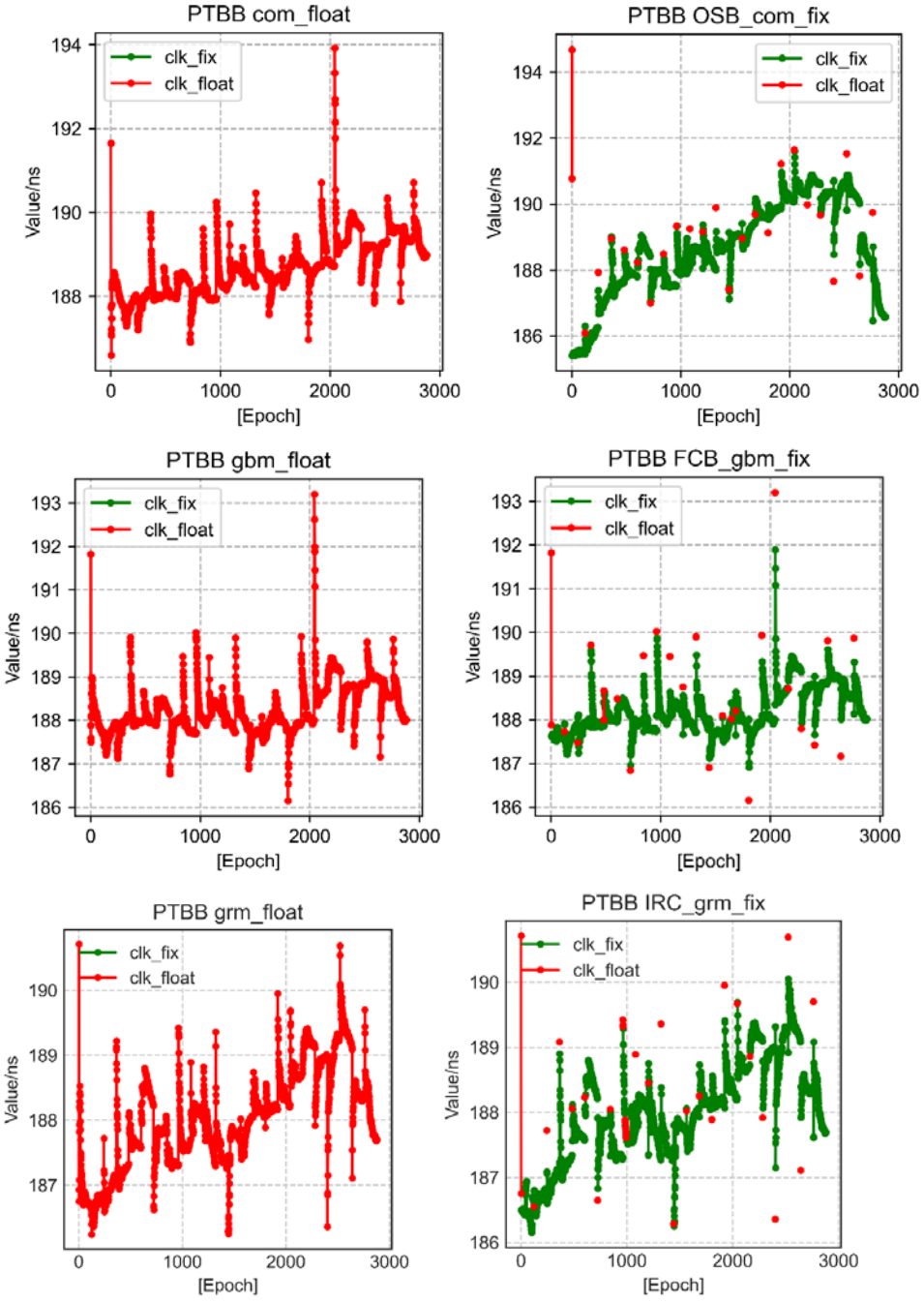

Preprints (www.preprints.org) | NOT PEER-REVIEWED | Posted: 24 October 2022 doi:10.20944/preprints202210.0349.v1

Figure 5. three strategies of PTBB station results with fixed and float ambiguity clock difference, where red represents floating point and green represents fixed solution.

No matter whatever fixing technique is employed, all of them are identical to the location and may successfully revert some points of clock discrepancy, as illustrated in Figure 5. What is the impact effect's magnitude? We examine them further.

We measure the STD box display of the 16 stations by comparing it to the final clock difference of the IGS week SNX file. Figure 6 illustrates how we confirmed our hypothesis that, with the exception of OSB_ com's fixed strategy, all other fixed strategies have lower STDs for clock difference fixed than the float solution.

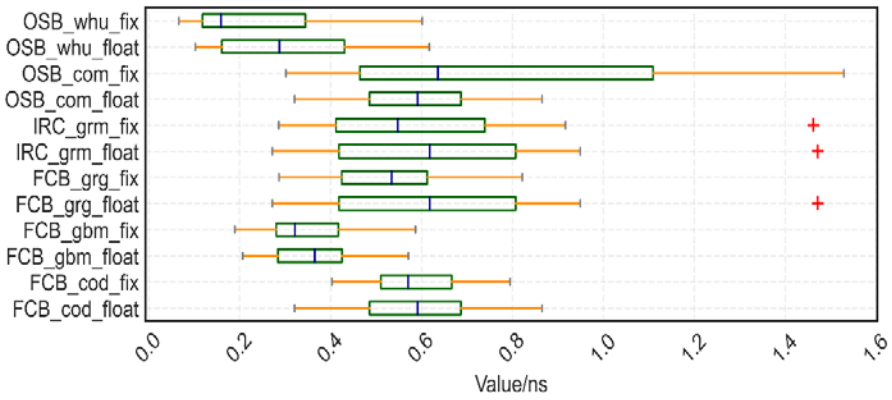

Figure 6. The STD box display of the 16 stations we choose to take the final clock difference of the IGS week SNX file as a reference, red"+" stands for outliers.

As the outcome of the clock difference improves, the event transfer also does, and we can now move on to the study of time linkages made up of two stations.

We create the 15 worldwide time comparison connections mentioned above using the PTBB station as the basis. Due to space restrictions, Figure 7 shows the sequence diagrams for the two time-links, PTBB-MGUE and PTBB-USN7. It is clear that fixed approach, particularly when using WHU goods, has a particular smoothing effect on unfixed.

We estimated the STD of the time transfer to assess the Type A uncertainty in the remote time transfer link using the time transfer results and calculation of station clock difference acquired from the IGS final product as a reference. For a single GPS, the time stability STD of time transfer is enhanced using various ambiguity-fixing procedures, and the improvement ranges from 10% to 40% in Figure 8's STD box display of 15 time-links. The one with the most improvement, up to 40%, is FCB_grm. OSB_com is the unconventional strategy. In the instance of a single station (Figure 6), one exception has already taken place, and a bigger exception follows the creation of the time
connection.

Preprints (www.preprints.org) | NOT PEER-REVIEWED | Posted: 24 October 2022 doi:10.20944/preprints202210.0349.v1

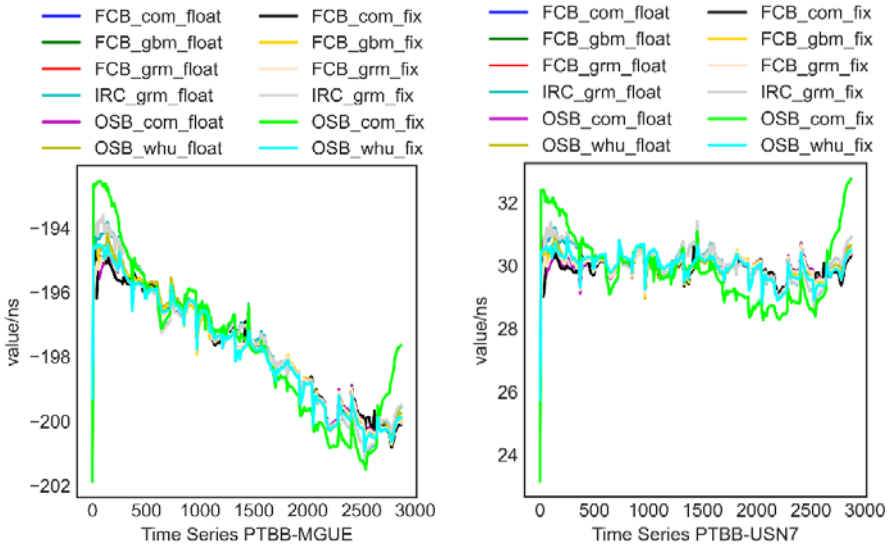

Figure 7. PTBB-MGUE/PTBB-USN7 Time links with different strategies.

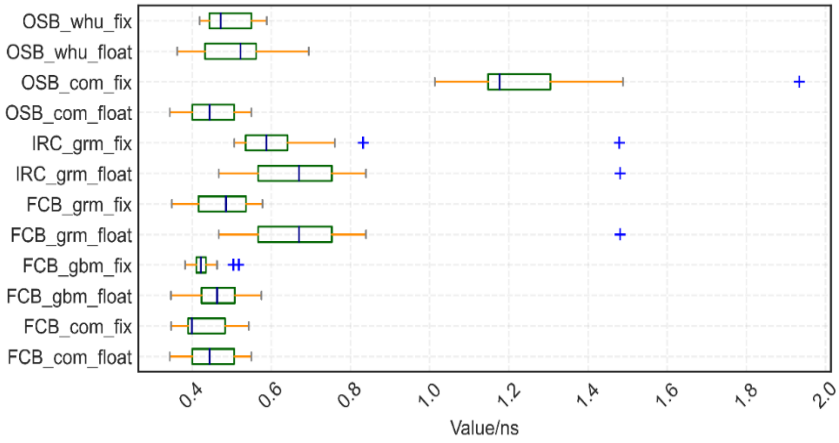

Figure 8. The STD box display of 15 time-links takes the final clock difference of the IGS week SNX file as a reference; blue"+" stands for outliers.

The frequency stability of the time-links between the PPP and PPPAR results should then be examined. The results of PPP and PPPAR are altering in the same manner for the transfer at the same moment (Figure.7). The PPPAR results' variability is minimal in comparison. We examine time linkages' frequency stability. To examine the frequency stability of time series, we employ the Allan variance modification technique and the following formula:

$$\delta_y^2(\tau)=\frac{1}{N-1}\sum_{i=1}^{N-1}\left(x_{n(k+1)-1}-2x_{nk+1}+x_{n(k-1)+1}\right)^2 \quad (20)$$

$$\operatorname{mod}\hat{\sigma}_y^2\left(n\cdot\tau_0\right)=\frac{1}{2n^4\tau_0^2(N-3n+1)}\sum_{j=1}^{N-3n+1}\left[\sum_{i=j}^{j+n-1}\left(x_{i+2n}-2x_{i+n}+x_i\right)\right]^2 \quad (21)$$

The above equation (20, 21), τ is the interval time, and the maximum can only be half of the number of data, x_n representing the phase data.

Preprints (www.preprints.org) | NOT PEER-REVIEWED | Posted: 24 October 2022 doi:10.20944/preprints202210.0349.v1

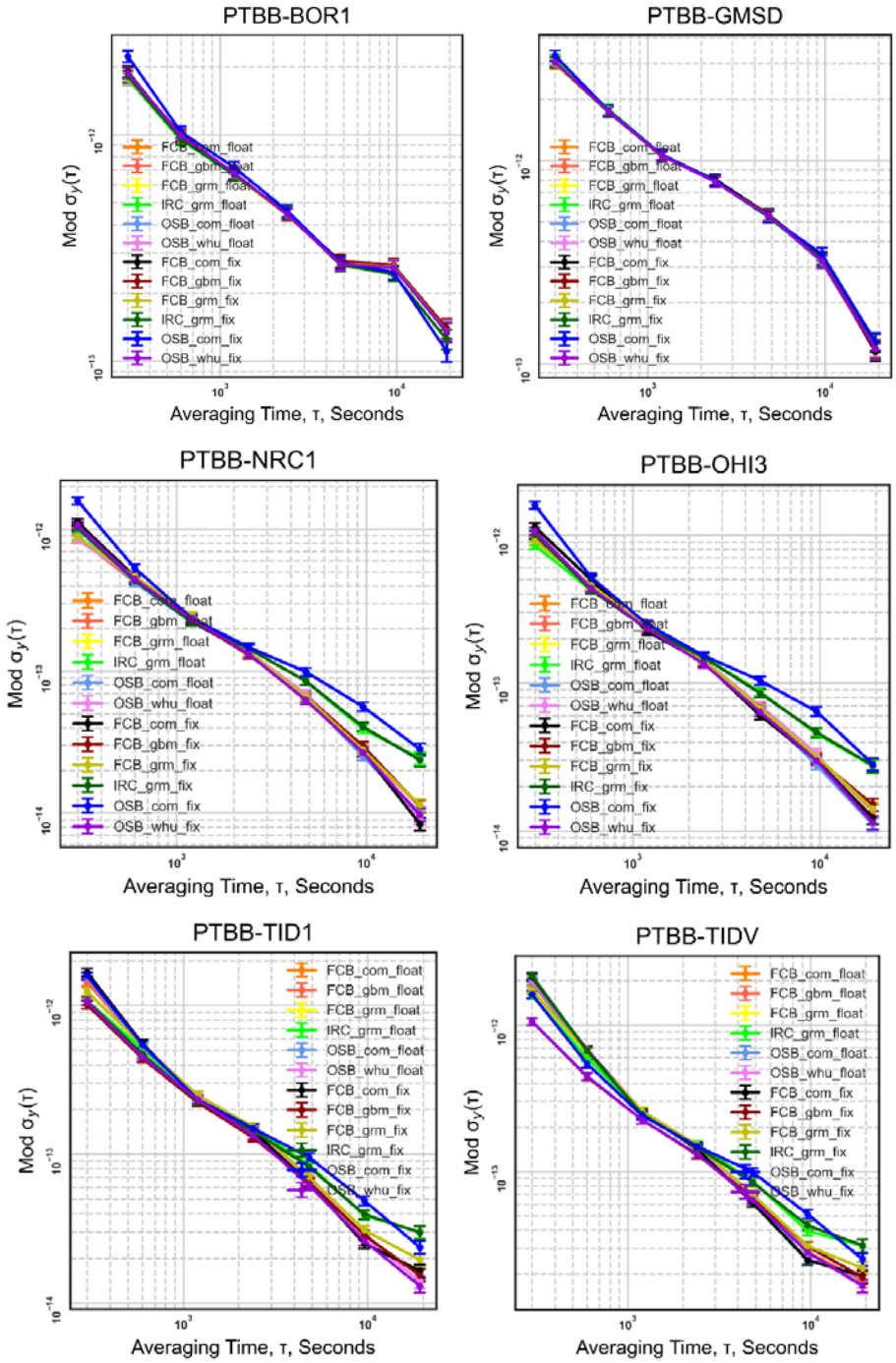

Figure 9. Frequency stability statistics of 6 time-links (PTBB-BOR1,PTBB-GMSD,PTBB-NRC1,PTBB-OHI3,PTBB-TID1,PTBB-TIDV)

Due to space constraints, we are only able to demonstrate the features of six common time-links (PTBB-BOR1, PTBB-GMSD, PTBB-NRC1, PTBB-OHI3, PTBB-TID1, PTBB-TIDV). Figure 9 makes it clear that the frequency stability of the time link has only slightly improved as a result of the ambiguity fixed technique. We discovered that between 1000 and 10,000 seconds, OSB com fix, IRC_ grm_ float, and IRC grm fix all perform poorly.

Preprints (www.preprints.org) | NOT PEER-REVIEWED | Posted: 24 October 2022 doi:10.20944/preprints202210.0349.v1

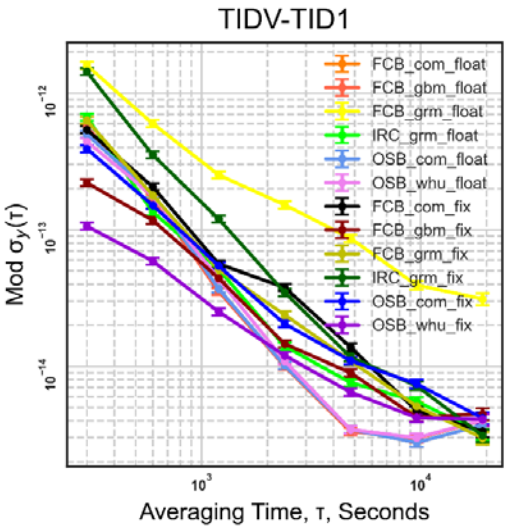

Figure 10. Frequency stability statistics of TIDV-TID1 time link with common clock.

Go one step further; in an ordinary clock time link, stations participating in time transfer share the same atomic clock. The relative clock skew from station to station will be eliminated. The standard can directly calculate the deviation to evaluate the time transfer performance. Taking TIDV-TID1 as an example, as shown in Figure.10, we can't get the conclusion that its frequency stability of a ambiguity fixed is better than this float one within short-term stability.

3.2. Muti-GNSS

Researchers have carried out pertinent experiments. The results of the time-frequency transfer are enhanced by the multi-GNSS PPP approach [31]. This section's goal is to demonstrate this for the multi-GNSS PPPAR technique time transfer.

We developed six schemes and fifteen particular comparison methods, as indicated in Table 5, in accordance with various ambiguity-fixed strategies and the satellite system integrated into the product. Following a set strategy based division into FCB, IRC, and OSB, the products are then further categorized into six schemes. Additionally, there are 15 precise fixed methods in the bundled Satellite system. GEC denotes the addition of BDS based on GPS and Galileo. G indicates for single GPS. GE stands for GPS plus Galileo.

Table 5. 15 detailed fixed strategies for multi-system

FCB	FCB-com	FCB_com_fix_G
		FCB_com_fix_GE
	FCB-gbm	FCB_gbm_fix_G
		FCB_gbm_fix_GE
	FCB-grg	FCB_grm_fix_G
		FCB_grm_fix_GE
IRC	IRC-grm	IRC_grm_fix_G
		IRC_grm_fix_GE
		IRC_grm_fix_GEC
OSB	OSB-com	OSB_com_fix_G
		OSB_com_fix_GE
		OSB_com_fix_GEC
	OSB-whu	OSB_whu_fix_G
		OSB_whu_fix_GE
		OSB_whu_fix_GEC

Preprints (www.preprints.org) | NOT PEER-REVIEWED | Posted: 24 October 2022 doi:10.20944/preprints202210.0349.v1

With only a minimal addition of satellite systems, we used the same PPP ambiguity fixing approach as in the preceding section. In a similar manner, we solve 16 stations, create 15 time-links centered on PTBB, and determine the STD with respect to the clock difference of the IGS weekly solution stations. The outcomes are displayed in Figure 11.

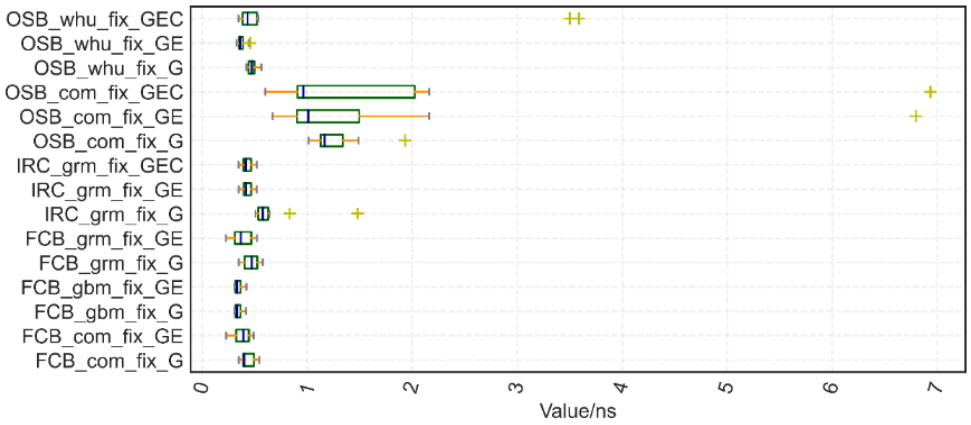

Figure 11. Muti-GNSS PPPAR time links STD concerning the clock difference of IGS weekly solution stations; yellow"+" stands for outliers.

As illustrated in Figure 11, with the exception of the COM product approach employing a single GPS, the statistical results of time link STD of PPPAR, whether single system or multi-system, can be maintained at the sub-nanosecond level; The six GE combinations have improved compared to the single GPS after the addition of the Galileo system, and the improvement ranges from 2% to 9%; The GEC combo has improved the majority of methods while weakening a few others. Inspection reveals that it is caused by some stations' subpar BDS fixes.

Preprints (www.preprints.org) | NOT PEER-REVIEWED | Posted: 24 October 2022 doi:10.20944/preprints202210.0349.v1

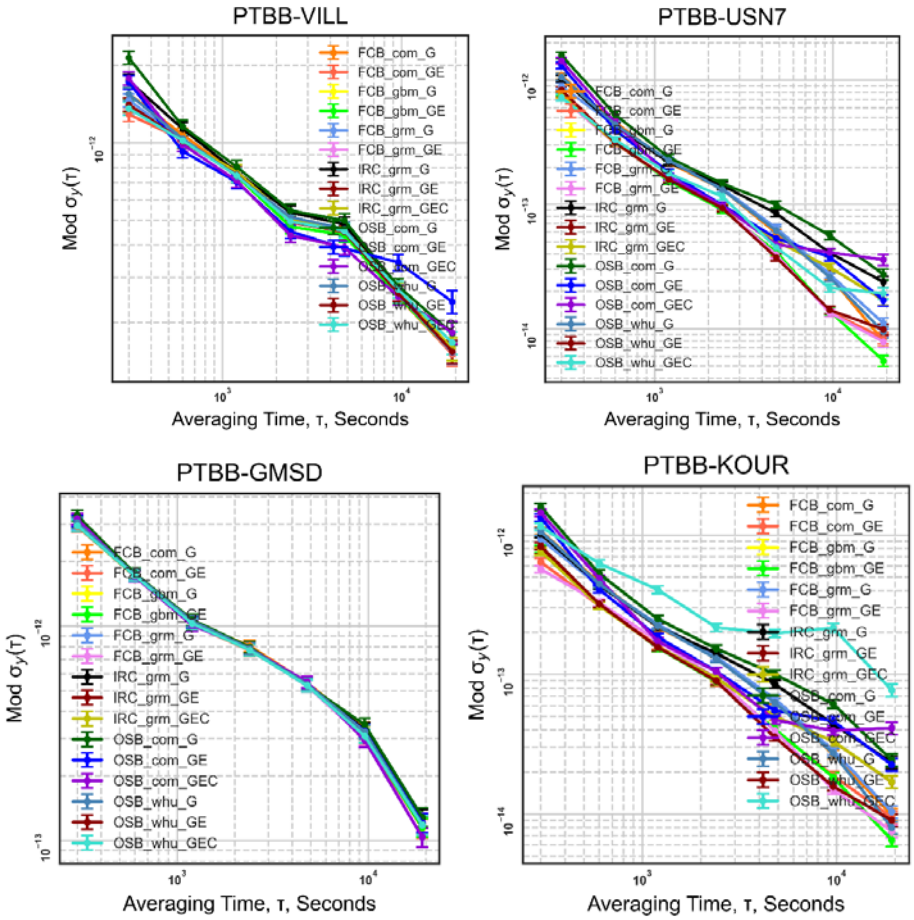

Figure 12. Frequency Stability statistics of Muti-GNSS PPPAR time links (PTBB-VILL, PTBB-USN7, PTBB-GMSD, PTBB-KOUR).

Due to physical constraints, we can only provide the frequency stability data of the four distinct Muti-GNSS PPPAR temporal links in Figure 12. The integration of multiple systems (Galileo, BDS) causes a significant shift in frequency stability, which is slightly different from the single system GPS. Even yet, some are weakened after being corrected, some are completely unaffected, and some are even better. We believe that despite the system's gain in short-term stability, the stability has not been greatly enhanced based on the comparison of multiple groups of linkages.

6. Conclusions

Different organizations and Analysis Centers (AC) offer various types of AR products using various methodologies. This paper chooses 16 MGEX stations with external high-precision atomic clocks to form 15-time comparison links and uses AR products data from CNES, SGG, CODE, and PRIDE laboratory. It then uses three ambiguity resolution strategies (FCB, IRC, OSB) to conduct high-precision time-frequency transfer experiments in order to thoroughly evaluate the impact of various strategies and AR products.

We arrive at the following findings by using the IGS end clock product as a reference and contrasting it with the float solution. With various ambiguity-fixing procedures, the time stability STD of time transfer is increased for a single GPS, and the improvement ranges from 10% to 40%. Of these, FCB_grm has undergone the greatest improvement, up to 40%; frequency stability has barely changed. When compared to a single GPS, combinations have improved with the addition of the Galileo system, and the improvements range from 2% to 9%. The majority of tactics have improved, while a few techniques have weakened with the GEC combination. We feel that the increase of the system within short-

 doi:10.20944/preprints202210.0349.v1

term stability has not significantly enhanced stability based on the comparison of multiple groups of links. This page serves as a great resource for PPPAR time-frequency transfer results in the future.

Author Contributions: Y.O., X.Z. conceived and designed the experiments; Y.O. performed the experiments, analyzed the data, and wrote the paper; X.Z., R.Y., and D.L. contributed to discussions and revisions. All authors have read and agreed to the published version of the manuscript."

Data Availability Statement: "Not applicable"

Acknowledgments: This work was supported by the National Key R&D Program of China (Grant No. 2021YFA0716500), the National Natural Science Foundation of China (Grant Nos. 61973328, 91938301), and the Key Basic Research Projects of Shenzhen Science and Technology Commission (Grant No.2020N259), and Shenzhen Science and Technology Program (Grant No.GXWD20201231165807008, 20200830225317001, ZDSYS20210623091807023)

Conflicts of Interest: The authors declare no conflict of interest."

 doi:10.20944/preprints202210.0349.v1

References

1. Zhang, H., M. Yan and W. Guang, Comparison of two-way and beidou common view time transfer between NTSC and BEIJ station. Advanced Materials Research, 2014. 1049-1050: p. 1997-2000.
2. Nawrocki, J., et al. An experiment of GPS+GLONASS common-view time transfer using new multi-system receivers. 2006: IEEE.
3. Allan, D.W. and M.A. Weiss. Accurate Time and Frequency Transfer During Common-View of a GPS Satellite. 1980: IEEE.
4. Harmegnies, A., P. Defraigne and G. Petit, Combining GPS and GLONASS in all-in-view for time transfer. Metrologia, 2013. 50(3): p. 277-287.
5. Petit, G. and Z. Jiang, GPS All in View time transfer for TAI computation. Metrologia, 2008. 45(1): p. 35-45.
6. Petit, G. and Z. Jiang, GPS All in View time transfer for TAI computation. Metrologia, 2007. 45(1): p. 35.
7. Petit, G. The TAIPPP pilot experiment. 2009: IEEE.
8. Victor Zhang, T.P.J.Y., Long-Term Uncertainty in Time Transfer Using GPS and TWSTFT Techniques. 2015.
9. Ray, J. and K. Senior, Geodetic techniques for time and frequency comparisons using GPS phase and code measurements. Metrologia, 2005. 42(4): p. 215-232.
10. Petit, G., et al., 1 × 10−16 frequency transfer by GPS PPP with integer ambiguity resolution. Metrologia, 2015. 52(2): p. 301-309.
11. Zumberge, J.F., et al., Precise point positioning for the efficient and robust analysis of GPS data from large networks. Journal of Geophysical Research Solid Earth, 1997. 102(B3): p. 5005-5017.
12. Su, K., S. Jin and Y. Ge, Rapid displacement determination with a stand-alone multi-GNSS receiver: GPS, Beidou, GLONASS, and Galileo. GPS solutions, 2019. 23(2): p. 1-12.
13. Lu, C., et al., Real-time retrieval of precipitable water vapor from GPS and BeiDou observations. Journal of geodesy, 2015. 89(9): p. 843-856.
14. Gao, Z., et al., Tightly coupled integration of multi-GNSS PPP and MEMS inertial measurement unit data. Gps Solutions, 2017. 21(2): p. 377-391.
15. Li, X., et al., Temporal point positioning approach for real-time GNSS seismology using a single receiver. Geophysical Research Letters, 2013. 40(21): p. 5677-5682.
16. Ge, M., et al., Resolution of GPS carrier-phase ambiguities in Precise Point Positioning (PPP) with daily observations. Journal of Geodesy, 2008. 82(7): p. 389-399.
17. Laurichesse, D. and F. Mercier, Integer Ambiguity Resolution on Undifferenced GPS Phase Measurements and its Application to PPP. Proceedings of International Technical Meeting of the Satellite Division of the Institute of Navigation, 2007: p. 839-848.
18. Collins, P., et al., Undifferenced GPS Ambiguity Resolution Using the Decoupled Clock Model and Ambiguity Datum Fixing. Navigation, 2010. 57(2): p. 123–135.
19. Shi, J. and Y. Gao, A comparison of three PPP integer ambiguity resolution methods. Gps Solutions, 2014.
20. Geng, J., et al., Integer ambiguity resolution in precise point positioning: method comparison. Journal of Geodesy, 2010. 84(9): p. 569-581.
21. Glaner, M. and R. Weber, PPP with integer ambiguity resolution for GPS and Galileo using satellite products from different analysis centers. GPS Solutions, 2021. 25(3).
22. Chen, C., et al., Assessment of GPS/Galileo/BDS Precise Point Positioning with Ambiguity Resolution Using Products from Different Analysis Centers. Remote sensing (Basel, Switzerland), 2021. 13(16): p. 3266.
23. Ouyang, M., et al., Research on time and frequency transfer during PPP convergence with parameters correlation comparison. Measurement, 2020: p. 108597.
24. Lyu, D., et al., Real-time clock comparison and monitoring with multi-GNSS precise point positioning: GPS, GLONASS and Galileo - ScienceDirect. Advances in Space Research, 2020. 65(1): p. 560-571.
25. Zhao, L., S. Ye and S. Jia, Handling the satellite inter-frequency biases in triple-frequency observations. Advances in Space Research, 2017. 59(8): p. 2048-2057.
26. Liu, S., et al., Tight integration of ambiguity-fixed PPP and INS: model description and initial results. GPS Solutions, 2016. 20(1): p. 39-49.
27. Defraigne, P., W. Aerts and E. Pottiaux, Monitoring of UTC(k)’s using PPP and IGS real-time products. GPS solutions, 2014. 19(1): p. 165-172.
28. Sastamoinen, J., Atmospheric correction for troposphere and stratosphere in radio ranging of satellites,in the Use of Artifical Satellites for Geodesy. Geophys.Monogr.Ser, 1972. 15.
29. Kou Ba, J., Testing of global pressure/temperature (GPT) model and global mapping function (GMF) in GPS analyses. Journal of Geodesy, 2009. 83(3-4): p. 199-208.
30. Petit, G. and B. Luzum, The IERS Conventions (2010). 2011.
31. Ge, Y., et al., Performance of Multi-GNSS Precise Point Positioning Time and Frequency Transfer with Clock Modeling. Remote Sensing, 2019. 11(3): p. 347.